Resonant Microwave Absorption in Thermally Deposited Au Nanoparticle Films Near Percolation Coverage

ARTICLE *in* LANGMUIR · JULY 2013

Impact Factor: 4.46 · DOI: 10.1021/la401753y · Source: PubMed

5 AUTHORS, INCLUDING:

Jan Obrzut
National Institute of Standards and Technology
21 PUBLICATIONS **609** CITATIONS
SEE PROFILE

J. F. Douglas
National Institute of Standards and Technology
428 PUBLICATIONS **14,879** CITATIONS
SEE PROFILE

James Alexander Liddle
National Institute of Standards and Technology
275 PUBLICATIONS **3,655** CITATIONS
SEE PROFILE

Langmuir

Article

pubs.acs.org/Langmuir

Resonant Microwave Absorption in Thermally Deposited Au Nanoparticle Films Near Percolation Coverage

Jan Obrzut,* Jack F. Douglas,* Oleg Kirillov, Fred Sharifi, and J. Alexander Liddle

National Institute of Standards and Technology, Gaithersburg, Maryland 20899, United States

ABSTRACT: We observe a resonant transition in the microwave absorption of thin thermally deposited Au nanoparticle films near the geometrical percolation transition p_c where the films exhibit a 'fractal' heterogeneous geometry. Absorption of incident microwave radiation increases sharply near p_c, consistent with effective medium theory predictions. Both the theory and our experiments indicate that the hierarchical structure of these films makes their absorption insensitive to the microwave radiation wavelength λ, so that this singular absorption of microwave radiation is observed over a broad frequency range between 100 MHz and 20 GHz. The interaction of electromagnetic radiation with randomly distributed conductive scattering particles gives rise to localized resonant modes, and our measurements indicate that this adsorption process is significantly enhanced for microwaves in comparison to ordinary light. In particular, above the percolation transition a portion of the injected microwave power is stored within the film until dissipated. Finally, we find that the measured surface conductivity can be quantitatively described at all Au concentrations by generalized effective medium theory, where the fitted conductivity percolation exponents and p_c itself are consistent with known two-dimensional estimates. Our results demonstrate that microwave measurements provide a powerful means of remotely measuring the electromagnetic properties of highly heterogeneous conducting films, enabling purposeful engineering of the electromagnetic properties of thin films in the microwave frequency range through fabrication of 'disordered' films of conducting particles such as metal nanoparticles or carbon nanotubes.

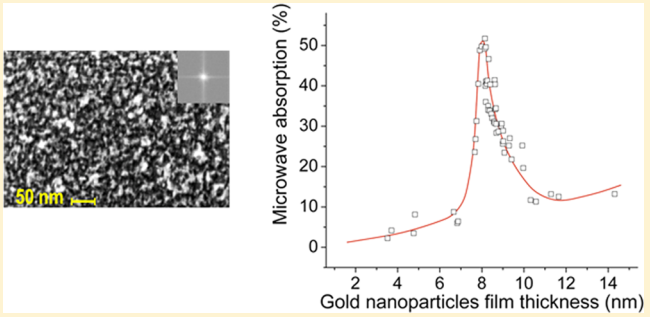

INTRODUCTION

Deposition of conducting particles onto dielectrically insulating interfaces or formation of semicontinuous metal films by thermal evaporation or sputtering can result in dramatic changes in the electromagnetic properties of the coated materials such as reflectivity and electrical conductivity.[1] Significant changes in electromagnetic response in these layers to various types of radiation, such as surface-enhanced Raman scattering,[2,3] Kerr effect,[4] and film reflectivity to visible, UV, and infrared radiation,[1,5] derive from the strong resonant interaction of the applied electromagnetic field with the complex morphology of these films. The strongest effects are generally expected to arise near the geometrical percolation threshold of metal coverage,[6,7] where the films have a highly fluctuating 'fractal' geometry involving hierarchically organized in-plane metal structures. This highly irregular film geometry is significant for '*anomalous*' absorption,[8,9] which has been observed near the percolation transition.[10,11] Although the nature of this interaction between the radiation and these metal films is yet not completely understood, it leads to local electromagnetic energy density field enhancements within film (hot spots) that exceed the incident field energy density by amplification factors as high as 10^5.[12−15]

There have been several previous studies emphasizing changes in the absorption of deposited metal films by light and infrared radiation, but microwave studies are scarce because of the inherent difficulty of such measurements.[16,17] The present paper focuses on development of new methods for making microwave scattering measurements on thin films. In particular, we measure conductance and absorption in the microwave frequency range for Au films in the vicinity of the percolation transition using a novel coplanar waveguide technique developed specifically for this purpose.[18] This method enables effective impedance matching and allows for accurate measurement of the film propagation characteristics. Our measurements directly confirm the predicted strong resonant interaction between the incident microwave radiation and the deposited Au film near percolation coverage. Encouragingly, we find that effective mean field theory[19,20] captures many aspects of our measurements. Scattering of electromagnetic waves from these generally disordered interfaces can be classified along with other critical phenomena derived from emergent interactions between particles exhibiting strong local interactions, and accordingly, we observe a striking singular absorption of microwave radiation near percolation coverage of Au that has not been seen before.

Received: May 7, 2013
Revised: June 18, 2013

EXPERIMENTAL METHODS

Film Preparation and Characterization. Thin semicontinuous films were deposited by thermal evaporation of gold directly onto CPWs through a shadow mask, leaving the corresponding reference CPWs uncoated. At the same time, we coated glass substrates for optical evaluation of the films. Evaporation was performed at a vacuum pressure of 10^{-4} Pa and at a deposition rate of 0.3 Å/s. Film mass thickness was monitored during deposition by a quartz crystal oscillator. Transmittance and reflectance spectra were measured at normal incidence over a wavelength of 0.3−2.5 μm using a Perkin-Elmer Lambda 950 UV−vis−NIR spectrophotometer equipped with a reflectance accessory kit for Lambda 950. Scanning electron microscope images were obtained using a Zeiss Supra 55 VP field emission SEM.

Fabrication of Coplanar Waveguide Testing Structure. Coplanar waveguides with a nominal characteristic impedance value (Z_0) of 50 Ω and a propagation length (l) ranging from 450 to 1800 μm were made with 10 nm Ti and 200 nm Au evaporated on 500 μm thick, 25 mm × 25 mm electronic-grade alumina wafers (Figure 1).

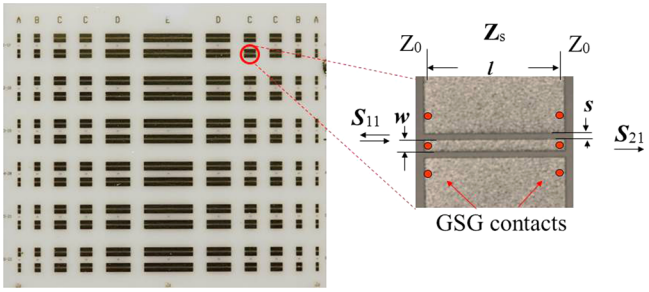

Figure 1. CPW wafer test structure (left), and geometry of a coplanar waveguide (right).

CPWs were patterned by contact lithography and lift. The width (w) of the central signal strip of these CPWs was 50 μm ± 0.2 μm, while the signal to ground plane spacing (s) was nominally 22 μm (Figure 1). In order to compensate for the manufacturing tolerances, the CPWs were arranged in several groups, each with ground plane spacing differing from the nominal value in steps of 1.0 μm, which covers Z_0 values from 49.0 to 51.0 Ω.

Microwave Measurement and Analysis. Measurements of the microwave wave scattering parameters, $\boldsymbol{S}_{11}$ and $\boldsymbol{S}_{21}$, were performed using an Agilent 8720D network analyzer in the frequency range from 1 to 20 GHz. The analyzer was connected to the CPW test structure with phase preserving cables from Agilent (85131−60013) and 50 Ω ground-signal-ground (GSG) air-coplanar probes (ACP-40, 100 μm pitch) from Cascade. The measurement system was calibrated using a 101C to 190C impedance calibration standard and WinCal calibration software from Cascade. Parameters in bold face denote complex quantities having both magnitude and phase.[18] After film deposition the CPW impedance changes from Z_0 to $\mathbf{Z}_s$. We consider the CPW test structure as a microwave network consisting of impedance discontinuity Z_0; $\mathbf{Z}_s$; $\mathbf{Z}_0$, that is, $\mathbf{Z}_s$ inserted between two reference transmission lines having a real characteristic impedance Z_0 where multiple wave reflection takes place at each Z_0; $\mathbf{Z}_s$ interface.[21] The material's properties in the specimen section of propagation length l are represented by the complex impedance $\mathbf{Z}_s$ and complex propagation constant $\boldsymbol{\gamma}_s$. The relation between the scattering parameters and the reflection coefficient, $\boldsymbol{\rho}_s$, and transmission coefficient $\boldsymbol{\tau}_s = e^{-\gamma_s l}$ is given by eqs 1a and 1b[21]

$$\boldsymbol{S}_{11} = \frac{\boldsymbol{\rho}_s(1 - e^{-\gamma_s l})(1 + e^{-\gamma_s l})}{1 - \boldsymbol{\rho}_s^2 e^{-2\gamma_s l}} \tag{1a}$$

$$\boldsymbol{S}_{21} = \frac{e^{-\gamma_s l}(1 - \boldsymbol{\rho}_s)(1 + \boldsymbol{\rho}_s)}{1 - \boldsymbol{\rho}_s^2 e^{-2\gamma_s l}} \tag{1b}$$

where $\boldsymbol{S}_{11}$ and $\boldsymbol{S}_{21}$ are the measured complex scattering parameters, $\boldsymbol{\gamma}_s$ is the complex propagation constant, and l is the propagation length. From eqs 1a and 1b one can find solutions for coefficients $\boldsymbol{\rho}_s$ and $\boldsymbol{\tau}_s$

$$\boldsymbol{\rho}_s = \boldsymbol{b} \pm \sqrt{\boldsymbol{b}^2 - 1}, \ \boldsymbol{b} = (\boldsymbol{S}_{11}^2 - \boldsymbol{S}_{11}^2 + 1)/(2\boldsymbol{S}_{11}) \tag{2a}$$

$$\boldsymbol{\tau}_s = e^{-\gamma_s l} = \left[\frac{1 - (\boldsymbol{S}_{11}/\boldsymbol{\rho}_s)}{1 - \boldsymbol{S}_{11}\boldsymbol{\rho}_s}\right]^{1/2} \tag{2b}$$

and

$$\mathbf{Z}_s = Z_0\left[\frac{(1 + \boldsymbol{S}_{11}) - \boldsymbol{S}_{21}^2{}^2}{(1 + \boldsymbol{S}_{11})^2\boldsymbol{S}_{21}^2}\right]^{1/2} \tag{2c}$$

Thus, the conductance, G_s, can be obtained from the conventional transmission line relation[19]

$$G_s = \mathrm{Re}\left(\frac{\gamma_s}{Z_s}\right) \tag{3}$$

and the absorption, A_s, is given by eq 4

$$A_s = 1 - T_s - R_s \tag{4}$$

where the transmission $T_s = \boldsymbol{\tau}_s\boldsymbol{\tau}_s^*$, reflectance $R_s = \boldsymbol{\rho}_s\boldsymbol{\rho}_s^*$, and $\boldsymbol{\tau}_s^*$ and $\boldsymbol{\rho}_s^*$ are the complex conjugate of the transmission and reflection coefficient, respectively.

The distributed conductance G_s (eq 3) can be correlated with the film surface conductance, $\sigma_s = G_s \cdot s/2$ (in units of Siemens per square), where (s) is the CPW signal to ground plane spacing, here s = 22 μm (Figure 1). By normalizing σ_s to the thickness (d) of the film, G_s can be scaled further to obtain the material's volume conductivity, $\sigma_v = \sigma_s/d$.

RESULTS

Examination of the semicontinuous gold films using scanning electron microscopy (SEM) reveals a granular structure with a surface morphology dependent on the average deposited film thickness (Figure 2). As in many past studies, we first see formation of islands that then coalesce into larger clusters with increasing film coverage. The film forms a connected or percolated network structure as more Au is deposited. The

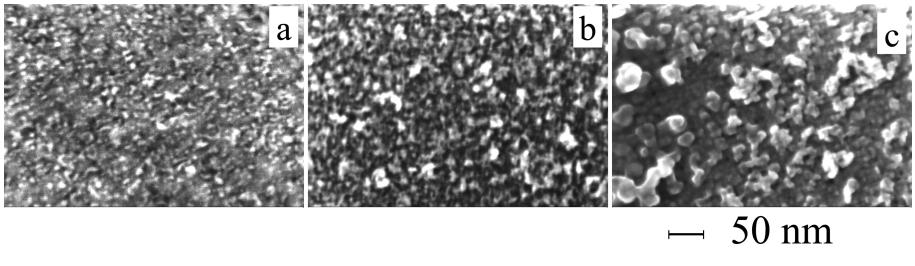

Figure 2. SEM images of thermally deposited Au films for films having a thicknesses of 4 (a), 7 (b), and 10 nm (c).

dx.doi.org/10.1021/la401753y | Langmuir XXXX, XXX, XXX−XXX

morphology becomes more hierarchical with increasing film thickness. From a radially averaged autocorrelation analysis of these SEM film images,[22] we estimate that the grain size within the percolation region (Figure 2b) to be about 20 nm for films 7 nm.

Conductivity Percolation in Microwave Frequency Range. The surface conductance σ_s measured in the frequency range from 100 MHz to 20 GHz is shown in Figure 3a for the

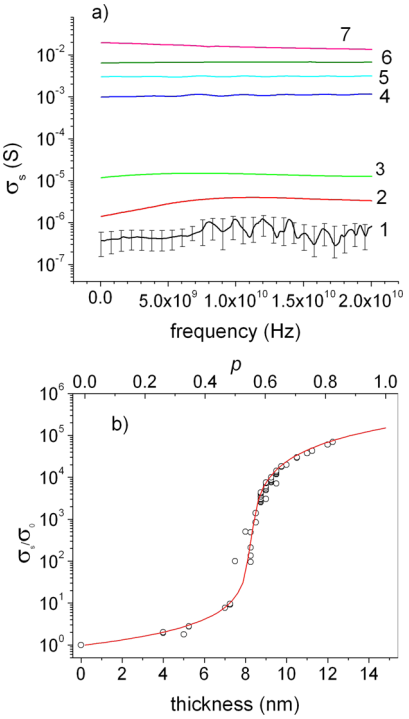

Figure 3. (a) Surface conductance (σ_s) for uncoated CPW (1) and CPWs coated with the following Au film thickness: (2) 4.0, (3) 7.0, (4) 8.0, (5) 8.5, (6)-9.0, and (7) 10.0 nm. Error bars shown in plot 1 for bare CPW are $\pm 2 \times 10^{-7}$ S/sq. (b) Relative surface conductance (σ_s/σ_0) at 10 GHz as a function of film thickness and particle area fraction, p. Solid line represents a fitting of GEM theory to our experimental data (circles).

alumina CPW substrate (plot 1) and for Au films (plots 2–7). Conductance is apparently frequency independent, a predicted characteristic of semicontinuous thin metallic films near p_c.[23] The surface conductance of the CPW substrate is approximately $(5 \pm 2) \times 10^{-7}$ S/sq. We assume this value to be the conductance of the insulating phase σ_0, the reference value of the conductivity in Figure 3b. As shown, the thinnest (4 nm) Au films are only weakly conducting, $\sigma_s = 4.0 \times 10^{-6}$ S/sq. Thicker films show considerably higher σ_s values with flat frequency characteristics. At 10 GHz, σ_s of a 7 nm thick film is about 1.4×10^{-5} S/sq, and this value increases further by 3 orders of magnitude to about 1.5×10^{-2} S/sq for films 10 nm thick. To verify that charge transport is confined to a nearly two-dimensional (2D) network, the conductivity σ_s of our thermally Au films in the microwave frequency range as a function of Au surface coverage p are fitted to the generalized effective medium theory (GEM).[20,24]

In previous work,[25] we applied GEM to model the conductivity of near two-dimensional layers of length-sorted single-wall carbon nanotubes (SWCNT) and found this theory to provide an excellent description of the conductivity of these nanoparticle layers with critical exponents governed by percolation theory. GEM theory captures the crossover between the high- and the low-conductivity states that is characteristic of most real composite materials. Figure 3b indicates that the Au film data is well described by this model over a wide range of Au concentrations. Here, we simply assumed a linear relation, $p = 0.068d$, between film thickness d (nm) and surface coverage, p.[1,8,10] We are not aware of a previous application of GEM theory to thermally deposited metal films. In the GEM model, the conductivity σ_s above p_c but close to the percolation threshold scales as $\sigma_s \approx \sigma_m (p - p_c)^t$, where t describes the singular changes in σ_s near the percolation threshold. In the fully covered film limit $p = 1.0$, we find the surface conductance to be about 5.2 S/sq, an appropriate value for a bulk metal.[1] Below p_c, we have the scaling $\sigma_s \approx \sigma_d (p_c - p)^s$ with an exponent s appropriate for the concentration range below p_c and the conductance of the pure dielectric σ_d designated $\sigma_d = \sigma_0$. From the GEM model fit to our data we determine that $\sigma_0 = 5 \times 10^{-7}$ S/sq, a percolation threshold coverage, $p_c \approx 0.54$, and the universal exponents t and s both have values of about 1.2 ± 0.2, close to the known "universal" percolation exponent values for these exponents in two dimensions.[20,26,27] Similarly, the p_c value of about 0.54 is consistent with the value of 0.5 predicted for a 2D square lattice.[28] Overall, these results are significant and consistent with two-dimensional charge transport. In comparison, $s \approx 0.73$ in three dimensions for thicker 20 nm films of random metallic particles.[29]

Microwave Reflectance, Transmittance, and Absorbance. Figure 4 shows the microwave reflectance $R_s = \boldsymbol{\rho}_s \boldsymbol{\rho}_s^*$, transmittance $T_s = \boldsymbol{\tau}_s \boldsymbol{\tau}_s^*$, and absorption A_s (eq 4) at 10 GHz plotted as a function of gold surface coverage, p. $\boldsymbol{\tau}_s^*$ and $\boldsymbol{\rho}_s^*$ are the complex conjugate of the microwave transmission and

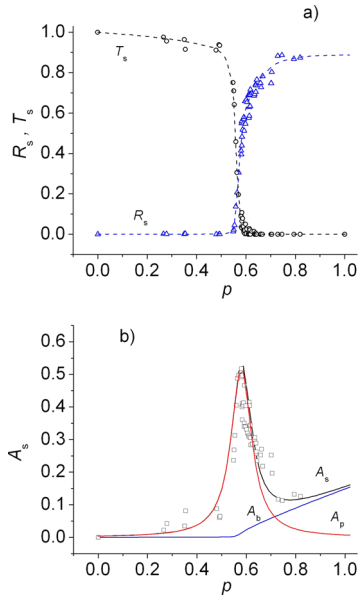

Figure 4. (a) Microwave reflectance (R_s, triangles) and transmittance (T_s, circles). (b) Absorption (A_s, squares) as a function of gold particle surface coverage p at frequency $f = 10$ GHz. Dashed lines in a are plotted through the points as guides to the eye. Solid lines in b are fitting results of absorption data (A_s) to the background-corrected absorption peak (A_p) defined through eq 5. Background absorption (A_b) is determined through eq 6 as attenuation of the electromagnetic power in terms of film conductivity and penetration depth.

dx.doi.org/10.1021/la401753y | Langmuir XXXX, XXX, XXX–XXX

reflection coefficients, respectively (eq 2a and 2b). We see that when the surface coverage $p < 0.5$ the reflectance is near zero. In this regime, the transmittance gradually decreases from 1.0 to about 0.9, which is balanced by a gradual increase in absorption, A_s. Within the percolation threshold, $p \approx p_c$, the transmittance falls rapidly to zero and A_s shows a narrow sharp peak reaching a maximum of about 0.5 while R_s increases steeply. Above the percolation transition, A_s decays, reaching a value of about 0.1, while R_s approaches a value of 0.9. The large value of reflectance above p_c is consistent with the Au film forming an electrically conducting mesh. Therefore, at a critical Au coverage we observe an insulator−conductor transition in the microwave response. We can roughly estimate the length scale of the heterogeneity in these films using scaling relations drawn from percolation theory. The percolation correlation length ξ_p obeys the scaling relation[11,30] $\xi_p \approx B\,(p - p_c)^{-\nu}$ with a size scaling exponent $\nu = 4/3$ in 2D, and we take the prefactor B to be on the order of unity. In our experiments the range of area fraction coverage over which the transition occurs is $\Delta p \approx 0.1$, the grain size $a \approx 20$ nm, giving a value of ξ_p of approximately 400 nm. The metallic mesh at wavelengths λ longer than ξ_p is almost totally reflecting, consistent with $R_s \approx 0.9$ as observed in Figure 4a. The dielectric contribution to the total reflection, which is typically observed at optical wavelengths as a linear increase of reflectance near the percolation transition[30] (see Figure 5), is negligible in Figure 4a. The narrow, essentially frequency-independent peak in Figure 4b provides evidence of resonant losses in the Au film near the microwave percolation transition. The peak has apparently Lorenzian shape typical for the resonant power damping. Since conductance, impedance, Z, and resistance, R, are frequency independent over a broad range of the particle surface concentrations, we can fit the microwave absorption data in Figure 4b to a sum of Lorenzian function A_p and background absorption A_b to describe the total absorption A_s over the percolation threshold

$$A_s = |R/Z| \frac{\chi}{\chi + (p - p_a)^2} + A_b \tag{5}$$

Here, $|R/Z|$ is the ratio of the internal film resistance and impedance,[31] χ is the peak width, and p_a is the peak position. The background contribution A_b to the total absorption A_s is derived from the wave attenuation due to film conductivity σ_v and the corresponding skin penetration depth, δ_p[32]

$$A_b = 1 - e^{-2\kappa d/\delta_p} \tag{6}$$

The constant 2 in eq 6 derives from the wave power damping relation rather than amplitude decay, d is the film thickness, and the parameter κ multiplies the wave damping distance for which we assume $1/\delta_p = (\pi f \mu_r \mu_0 \sigma_V)^{1/2}$.[32] We determined, $\sigma_v = \sigma_s/d$ from our GEM percolation conductivity fitting results for each d. The fitted parameter $\kappa = 5.9$ therefore in the semicontinuous film the effective attenuation distance of microwaves is longer by a factor of about 5.9 compared to the film thickness. The fitted peak position $p_a \approx 0.58$ is slightly above the percolation threshold.

Optical Reflectance, Transmittance, and Absorbance. In comparison to the microwave range, reflectance (R), transmittance (T), and absorption (A) of semicontinuous gold films at optical frequencies show different characteristics (Figure 5). The most striking difference is seen in the percolation transition region where R increases linearly vs p

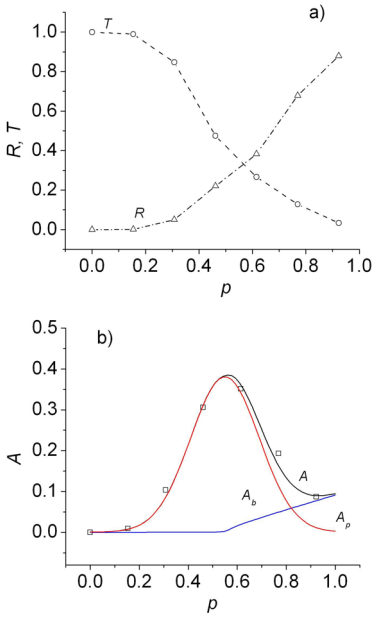

Figure 5. (a) Optical reflectance (R, triangles) and transmittance (T, circles). (b) Absorption (A, squares) as a function of gold particle surface coverage (p) at a wavelength λ of 2.5 μm. Dashed lines in a are plotted through the points as guides. Solid lines in b represent fit of the background corrected absorption data (A_{op}) to a Gaussian function where the background absorption (A_{ob}) is defined in terms of the film absorption coefficient, α.

while absorbance shows a broad peak spanning from $p \approx 0.3$ to $p \approx 0.7$. Near the percolation threshold, R approaches a value of about 0.3, $A \approx 0.4$, while $T \approx 0.3$, that is the film is still 30% transparent. When corrected for background absorption due to resistive losses the peak assumes a symmetric Gaussian-like shape.[33] We approximated the optical background absorption A_b by fitting it to an absorption function given by eq 6, $A_b = 1 - e^{-2ad}$. The absorption coefficient $\alpha = 1/\delta p = (\pi f \mu_r \mu_0 \sigma_{vo})^{1/2}$ is expressed by the skin penetration depth[32] δ_p, which at optical wavelengths depends on the film optical conductivity σ_{vo}. We estimated the optical conductivity of our films at λ of 2.5 μm (frequency, $f = 1.2 \times 10^{14}$ Hz) from our GEM conductivity percolation fitting results shown in Figure 3b where we assumed simple Drude oscilator model.[34,35]

We find that σ_{vo} values are smaller than the microwave σ_v at 10 GHz by a factor of 10^3, in fairly good agreement with the available experimental data measured at in the THz range.[1] In Figure 5b, the peak position is about 0.54, the peak amplitude is 0.38, and the optical absorption coefficient at p_c $\alpha \approx 0.001$ nm^{-1}. The width of the absorption peak deconvoluted from the optical absorption data $\Delta p = 0.3$, which is over three times wider than in the microwave rage, where at $\lambda \approx 3$ cm $\Delta p = 0.1$. Evidently, the width Δp of the percolation transition increases with decreasing wavelength, consistent with effective medium theory.[12,33]

DISCUSSION

The optical peak absorption has been attributed to large local field fluctuations which have been modeled through several techniques,[2,8,9,12] including the effective medium theory.[33] The optical conductivity attenuates the electric field in a random network of a Drude metal. The primary assumption behind these theoretical efforts is that the skin penetration depth at percolation is much smaller locally than the metallic grain

dx.doi.org/10.1021/la401753y | Langmuir XXXX, XXX, XXX−XXX

size.[9,12−15,36,37] Indeed, the transmittance of these thin films falls far more rapidly within the percolation transition than the classical skin depth model would suggest.[1,17] Above the percolation transition in the metallic range, we find the optical absorption coefficient α is consistent with the conductivity of the Drude metal at $\lambda = 2.5\ \mu m$ (1.2×10^5 GHz).

Our microwave scattering experimental data suggest that the interaction of radiation with randomly distributed conductive particles leads to localized resonant modes within the film, where the resonant wave is confined to a dimension comparable with the percolation correlation length rather than the film thickness. In an attempt to explore the origin of the microwave absorption in more detail we examine the phase characteristic of the reflected wave, S_{11}. Figure 6 indicates that

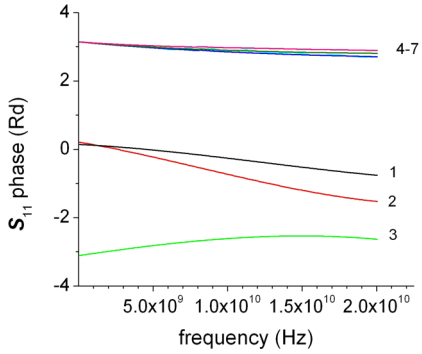

Figure 6. Phase angle of the microwave scattering parameter S_{11} for uncoated CPW (1) and the following Au film thickness: (2) 4.0, (3) 7.0, (4) 8.0, (5) 8.5, (6) 9.0, and (7) 10.0 nm.

below the percolation threshold the phase angle (φ) of the scattering parameter S_{11} is negative, consistent with the predominantly dielectric character of the film.

With increasing film thickness beyond the percolation threshold the phase angle changes from negative to positive values by about π. This indicates a transition from the capacitive (X_C) to the inductive reactance (X_L), evidencing a quarter-wavelength resonance, which leads to resonant power dissipation. The film response is equivalent to an electrically shorted transmission line length of $\lambda_g/4$. The guided wavelength $\lambda_g = \lambda_0/(\varepsilon_r)^{0.5}$ is shorter than the incident free space wavelength λ_0 by a factor of the effective relative dielectric constant $(\varepsilon_r)^{0.5}$. In randomly distributed metallic and dielectric clusters ε_r diverges near p_c[38,39] and may locally increase over several orders of magnitude,[12,37,39] compressing λ_g to a length scale comparable with the percolation correlation length ξ_p. By tuning the particle concentration toward p_c the structure of the semicontinuous film transitions from an electric to magnetic energy concentrator.

As discussed earlier, our results indicate that the effective attenuation distance of microwaves in semicontinuous film is longer by a factor of about 5.9 than the film thickness and comparable to twice the average grain size. In the case of the 7 nm thick films, which have an average grain size of ≈20 nm (Figure 2b), the effective attenuation distance is about 40 nm. This result quantifies absorption of semicontinuous films above percolation and clarifies its considerably higher value compared to continuous metallic films. In eq 5 $|R/Z|$ is the ratio of the internal film resistance and impedance, which normalizes the resonant absorption (Figure 4b, plot A_p) such that when $Z = R$, $A_s = 1.0$.[31] We see that when A_p attains a maximum value ≈ 0.5, the film reactance is inductive ($Z = R + X_L$, Figure 6) and $R/(R + X_L) \approx 0.5$, and therefore, a significant portion of the injected microwave power is stored in the magnetic field until dissipated. This result indicates that it is possible to strongly modulate the storage microwave energy in semicontinuous films through control of the nanoscale film morphology. It is remarkable that such thin films can change the electromagnetic response so profoundly, even away from the percolation threshold. The ordinary effective medium theory applied to optical range predicts the absorption peak to have a near Gaussian form rather than Lorenzian after background subtraction. We believe that this more singular Lorenzian behavior will naturally arise from the GEM theory applied to electromagnetic scattering, which is a more suitable model for materials having a high-conductivity contrast. Such theoretical approach has not been successfully developed yet, and we employed a resonant circuit model approximation to describe the microwave absorption quantitatively.

Recent studies have shown that it is possible to fully cloak rod-like dielectric structures of moderate cross-section to radiofrequency radiation by coating these objects with thin conductive layers ('mantle coating'), an effect along the same line of the results of the present paper where the microwave radiation can be intensely absorbed.[40] Strong absorption of incident radiation in the microwave region has also been observed in dielectric rods whose surfaces have been decorated with metallic strips, demonstrating proof of principle for a robust cloaking effect.[41] Our own work seems to indicate that similarly strong adsorption of microwave and corresponding metamaterial applications should be possible when the coating layers have ultrathin nanometric film thicknesses.

CONCLUSION

In summary, we present a new technique to effectively allow coupling of microwaves to nanostructured films over a broad frequency range. We find strong evidence that large resonant absorption of the gold layer near the geometrical percolation threshold leads to a sharp insulator−metal transition where the change of the interfacial conductivity can be precisely described by the percolation theory in two dimensions. Our results indicate that the effective attenuation distance of microwaves in semicontinuous film is longer than the film thickness and comparable to twice the film average grain size. The films attain a maximum absorption of about 0.5, slightly above the percolation threshold (p_c). By increasing the particle concentration toward p_c the film reactance becomes inductive and the structure transitions from an electric to a magnetic energy concentrator. The presented analysis allows for more detailed studies of the mechanism of microwave absorption, and it should then be possible to differentiate among several physical processes that have been suggested for the intense interaction of the electromagnetic field with these disordered films. The effect also opens the possibility of manipulating microwave energy in subwavelength structures through engineering the fine structure of metallic films. The presented microwave experiment can be a powerful measurement tool for thin films of deposited conducting nanoparticles layers such as metal nanoparticles and carbon nanotubes, etc., that could be used in the design and process characterization of microwave reflective surfaces and devices that use this effect.

dx.doi.org/10.1021/la401753y | Langmuir XXXX, XXX, XXX−XXX

AUTHOR INFORMATION

Corresponding Author

*E-mail: jan.obrzut@nist.gov, jack.douglas@nist.gov.

Notes

The authors declare no competing financial interest.

ACKNOWLEDGMENTS

This work was supported in part by a research grant from the NIST Center of Nanoscience and Technology.

REFERENCES

(1) Thoman, A.; Kern, A.; Helm, H.; Walther, M. Nanostructured Gold Films as Broadband Terahertz Antireflection Coatings. *Phys. Rev. B* **2008**, *77*, 195405.

(2) Brauers, F.; Blacher, S.; Lagarkov, A. N.; Sarychev, A. K.; Gadenne, P.; Shalev, V. M. Theory of giant Raman scattering from semicontinuous metal films. *Phys. Rev. B* **1997**, *57*, 13234−13244.

(3) Gadenne, P.; Brauers, F.; Shalev, V. M.; Sarychev, A. K. Giant Stokes fields on semicontinuous metal films. *J. Opt. Soc. Am. B* **1998**, *15*, 68−72.

(4) Shalev, V. M.; Sarychev, A. K. Nonlinear optics of random metal-dielectric films. *Phys. Rev. B* **1998**, *57*, 13285−13288.

(5) Stockman, M. I. Nanoplasmonics: Past, Present, and Glimpse into Future. *Opt. Express* **2011**, *19*, 22029−22106.

(6) Bergman, D. J.; Imry, Y. Critical Behavior of the Complex Dielectric Constant near the Percolation Threshold of a Heterogeneous Material. *Phys. Rev. Lett.* **1977**, *39*, 1222−1225.

(7) Peng, Y.; Paudel, T.; Chen, W. -C; Padilla, W. J.; Ren, Z. F.; Kempa, K. Percolation and Polaritonic Effects in Periodic Planar Nanostructures Evolving from Holes to Islands. *Appl. Phys. Lett.* **2010**, *97*, 041901.

(8) Robin, Th.; Souillard, B. Anomalous Infrared Absorption of Granular Films near the Percolation Threshold: A Microscopic Approach. *Opt. Commun.* **1989**, *71*, 15−19.

(9) Sarychev, A. K.; Bergman, D. J.; Yagil, Y. Theory of the optical properties of metal-dielectric films. *Phys. Rev. B* **1995**, *51*, 5366−5385.

(10) Yagil, Y.; Gadenne, P.; Julien, C.; Deutscher, G. Optical properties of thin semicontinuous gold films over a wavelength range of 2.5 to 500 μm. *Phys. Rev. B* **1992**, *46*, 2503−2511.

(11) Berthier, S.; Peiro, J. Anomalous Infrared Absorption of Nanocermets in the Percolation Range. *J. Phys.: Condens. Matter* **1998**, *10*, 3679−3694.

(12) Shubin, V. A.; Sarychev, A. K.; Clerc, J. P.; Shalev, V. M. Local Electric and Magnetic Fields in Semicontinuous Metal Films: Beyond the Quasistatic Approximation. *Phys. Rev. B* **2000**, *62*, 11230−11244.

(13) Ducourtieux, S.; Podolskiy, V. A.; Grésillon, S.; Buil, S.; Berini, B.; Gadenne, P.; Boccara, A. C.; Rivoal, J. C.; Bragg, W. D.; Banerjee, K.; Safonov, V. P.; Drachev, V. P.; Ying, Z. C.; Sarychev, A. K.; Shalaev, V. M. Near-field optical studies of semicontinuous metal films. *Phys. Rev. B* **2001**, *64*, 165403.

(14) Krachmalnicoff, V.; Castanie, E.; Widde, Y. De; Carminati, R. Fluctuations of the Local Density of States Probe Localized Surface Plasmons in Disordered Metal Films. *Phys. Rev. Lett.* **2010**, *105*, 183901−183901−4.

(15) Pavaskar, P.; Theiss, J.; Cronin, S. B. Plasmonic Hot Spots: Nanogap Enhancement vs. Focusing Effects from Surrounding Nanoparticles. *Opt. Express* **2012**, *20*, 14656−14662.

(16) Lagarkov, A. N.; Rozanov, K. N.; Sarychev, A. K.; Simonov, N. A. Experimental and Theoretical Study of Metal-Dielectric Percolating Films at Microwaves. *Physica A* **1997**, *241*, 199−206.

(17) Hooper, I. R.; Sambles, J. R. Some Considerations on the Transmissivity of Thin Metal Films. *Opt. Express* **2008**, *16*, 17249−17257.

(18) Obrzut, J.; Kirillov O. Microwave Conductance of Semicontinuous Metallic Films from Coplanar Waveguide Scattering Parameters. *2013 IEEE International Instrumentation and mesurement Technology Conference Proceedings*, Minneapolis, MN, May 6−9, 2013, pp 912−916.

(19) Staufer, D.; Aharony, A. *Introduction to Percolation Theory*; Taylor & Francis: Washington, D.C., 1992.

(20) Sahimi, M. *Heterogeneous Materials I: Linear Transport and Optical Properties*; Springer: New York, 2003.

(21) Obrzut, J. General Analysis of Microwave Network Scattering Parameters for Characterization of Thin Film Materials. *Measurement J.* **2013**, DOI: 10.1016/j.measurement.2013.04.049.

(22) Wang, D.; Shaaf, P. Nanoporous Gold nanoparticles. *J. Mater. Chem.* **2012**, *22*, 5344−5348.

(23) Brouers, F.; Clerck, J. P.; Giraud, G. Dielectric and Optical Properties close to the Percolation Threshold. *Phys. Rev. B* **1991**, *44*, 5299−5302.

(24) McLachlan, D. S.; Sauti, G.; Chiteme, C. Static Dielectric Function and Scaling of the AC Conductivity for Universal and Nonuniversal Percolation Systems. *Phys. Rev. B* **2007**, *76*, 014201.

(25) Simien, D.; Fagan, J. A.; Luo, W.; Douglas, J. F; Migler, K.; Obrzut, J. Influence of Nanotube Length on the Optical and Conductivity Properties of Thin Single-Wall Carbon Nanotube Networks. *ACS Nano* **2008**, *2*, 1879−1884.

(26) Sahimi, M.; Hughes, B. D.; Scriven, L. E.; Davis, H. T. Critical Exponents of Percolation Conductivity by Finite Size Scaling. *J. Phys. C: Solid State Phys.* **1983**, *16*, L521−L527.

(27) Mertens, S.; Moore, C. Continuum Percolation Thresholds in Two Dimensions. *Phys. Rev. E* **2012**, *86*, 061109−061109−6.

(28) Galam, S.; Mauger, A. Universal Formulas for Percolation Threshold. *Phys. Rev. E* **1996**, *53*, 2177−2181.

(29) Grannan, D. M.; Garland, J. C.; Tanner, D. B. Critical Behavior of the Dielectric Constant of a Random Composite near the Percolation Threshold. *Phys. Rev. Lett.* **1981**, *46*, 375−378.

(30) Robin, Th.; Souillard, B. A Microscopic Theory of the Reflection Properties of Metal-Insulator Composite Films. *Physica A* **1993**, *193*, 79−104.

(31) Sucher, M. Measurement of Q. In *Handbook of Microwave Measurements, Microwave Measurements*; Sucher, M., Fox, J., Eds.; Polytechnic Press of the Polytechnic Institute of Brooklyn: New York, 1963; p 420.

(32) Ramo, S.; Whinnery, J. R.; Van Duzer, T. *Fields and Waves in Communication Electronics*; Wiley: New York, 1994; p 151.

(33) Brouers, F.; Clerck, J. P.; Giraud, G.; Laugier, J. M.; Randrimantany, Z. A. Dielectric and Optical Properties close to the Percolation Threshold II. *Phys. Rev. B* **1993**, *47*, 666−673.

(34) Smith, G. B.; Maaroof, A. I.; Gentle, A. Homogenized Lorenz-Drude Optical Response in Highly Nanoprous Conducting Gold Layers Produced by de-Alloying. *Opt. Commun.* **2007**, *271*, 263−268.

(35) Hovel, M.; Gompf, B.; Dressel, M. Dielectric Properties of Metal Films Around the Percolation Threshold. *Phys. Rev. B* **2010**, *81*, 035402.

(36) Brauers, F.; Blacher, S.; Sarychev, A. K. Giant Field Fluctiuations and Anomalous Light Scattering from Semicontinuous Metal Films. *Phys. Rev. B* **1998**, *58*, 15897−15903.

(37) Seal, K.; Sarychev, A. K.; Noh, H.; Genov, D. A.; Yamilov, A.; Shalaev, V. M; Ying, Z. C.; Cao, H. Near-Field Intensity Correlations in Semicontinuous Metal-Dielectric Films. *Phys. Rev. Lett.* **2005**, *94*, 226101.

(38) Efros, A. L.; Sklovsii, B. I. Critical Behavior of Conductivity and Dielectric Constant near the Metal-Non-Metal transition Threshold. *Phys. Status Solidi B* **1976**, *76*, 475−485.

(39) Wu, R. F.; Pan, W.; Shi, S. L.; Han, R. B. Critical Behaviors of the Conductivity and Dielectric Constant of Ti3SiC2/Al2O3 Hybrids. *J. Appl. Phys.* **2007**, *102*, 056104.

(40) Rainwater, D.; Kerkhoff, A.; Soric, J. C.; Moreno, G.; Alu, A. Experimental Verification of Three-Dimensional Cloaking in Free-Space. *New J. Phys.* **2012**, *14*, 013054.

(41) Soric, J. C.; Chen, P. Y.; Kerkhoff, A.; Rainwater, D.; Melin, K.; Alu, A. Demonstration of an Ultralow Profile Cloak for Scattering suppression of a Finite-Length Rod in Free Space. *New J. Phys.* **2013**, *15*, 033037.